INTERNATIONAL JOURNAL OF CLIMATOLOGY
*Int. J. Climatol.* **37**: 4027–4042 (2017)
Published online 6 January 2017 in Wiley Online Library
(wileyonlinelibrary.com) DOI: 10.1002/joc.4983

RMetS
Royal Meteorological Society

# A statistical analysis of hourly heavy rainfall events over the Beijing metropolitan region during the warm seasons of 2007–2014

Huiqi Li,[a,b] Xiaopeng Cui[a,b,c]* and Da-Lin Zhang[d,e]

[a] *Key Laboratory of Cloud-Precipitation Physics and Severe Storms, Institute of Atmospheric Physics, Chinese Academy of Sciences, Beijing, China*
[b] *College of Earth Science, University of Chinese Academy of Sciences, Beijing, China*
[c] *Collaborative Innovation Center on Forecast and Evaluation of Meteorological Disasters, Nanjing University of Information Science and Technology, China*
[d] *State Key Laboratory of Severe Weather, Chinese Academy of Meteorological Sciences, Beijing, China*
[e] *Department of Atmospheric and Oceanic Science, University of Maryland, College Park, MD, USA*

**ABSTRACT:** A statistical analysis of the spatiotemporal characteristics of hourly heavy rainfall (HHR) events and rainstorm days, defined as greater than 20 mm $h^{-1}$ and 50 mm $day^{-1}$, respectively, is performed using observations at 5-min intervals from 155 automated weather stations (AWSs) over the Beijing metropolitan region (BMR) during the warm seasons of 2007–2014. Results show pronounced variability in the frequencies and rainfall amounts of both HHR events and rainstorm days across the BMR of less than 150 km width from the west to east. That is, higher- (lower) frequency HHR events with more (less) accumulated rainfall amounts take place in eastern Haidian and over the BMR's northeast mountains (west and northwest mountains). Many extreme rainfall and even record-breaking events, in terms of the frequency, duration, rainfall amount and intensity, are found to occur in the regions of high-frequency HHR events and rainstorm days. The frequency of rainstorm days with HHR events accounts for more than 50% of that of total rainstorm days over the BMR's plains and near the northeast mountains. Results also show that HHR events occur most frequently in late July, and typically peak during 1600–2000 LST. A comparison of the averaged surface meteorological variables and upper-air sounding at 0800 LST between HHR and non-HHR days reveals that the occurrences of the HHR events coincide with the distribution of surface warmer and more humid air as well as organized convergence in the presence of an unstable environment with surface south- to southeasterly winds, low-level south to southwesterly flows and a deep layer of higher moisture content. These results suggest likely the positive influences of urban environment and mountain-plain circulations on the generation of the HHR events, given favourable larger-scale conditions.

KEY WORDS hourly heavy rainfall; rainstorm days; extreme rainfall

*Received 21 January 2016; Revised 25 November 2016; Accepted 5 December 2016*

## 1. Introduction

The Beijing metropolitan region (BMR) has experienced heavy rainfall events exceeding 20 mm $h^{-1}$ from time to time during warm seasons (i.e. from 1 May to 30 September), resulting often in severe urban flooding, and landslides in the BMR's mountainous regions. One of the most recent extreme rainfall events occurred on 21 July 2012 (Zhang *et al.*, 2013; Zhong *et al.*, 2015), the so-called 7–21 extreme rainfall event in China, when over 120 BMR's automated weather stations (AWSs) recorded hourly rainfall amounts exceeding 20 mm. This extreme heavy rainfall event left 79 people dead and caused nearly $2 billion direct economic losses. Since such heavy rainfall events with hourly rainfall amounts exceeding 20 mm occur more abruptly, it is hard to predict their timings and locations by both operational numerical weather prediction models and experienced forecasters, often leaving the local governments and public unprepared. Thus, more attention has recently been paid to the development and prediction of hourly heavy rainfall (HHR) events.

There have been numerous case studies of short-duration heavy rainfall events over the BMR during the past decades (e.g. Wang *et al.*, 2003; Sun *et al.*, 2006; Liu *et al.*, 2007; Sun and Yang, 2008; Zhang *et al.*, 2012). A few statistical studies have also been conducted to study different aspects of rainfall over the BMR but with limited available data. For example, Li *et al.* (2008) used hourly self-recording rain-gauge data at a station located at the BMR's southern suburban to study the diurnal cycle of summer rainfall and found two peaks occurring in the late afternoon and early morning hours, respectively. Li *et al.* (2011) analysed hourly rain gauge records in the late summer months of 1966–2005, and found that 1–6 h rainfall events decreased in frequency but increased in intensity

* Correspondence to: X. Cui, Key Laboratory of Cloud-Precipitation Physics and Severe Storms, Institute of Atmospheric Physics, Chinese Academy of Sciences, Beijing 100029, China. E-mail: xpcui@mail.iap.ac.cn

whereas longer-duration rainfall events decreased in both frequency and amount. Yin *et al.* (2011) found that the BMR's plain and mountainous areas exhibited a night and an afternoon peak of summer rainfall, respectively, based on hourly rainfall data from 26 AWSs in the BMR and Hebei Province. Recently, with hourly rainfall data from the BMR's 123 AWSs, Liu *et al.* (2014) analysed the monthly rainfall variations from April to October, and found that the peak monthly rainfall and the highest hourly rainfall intensity occurred in July. Of significance is that Yang *et al.* (2013, 2016), Liu *et al.* (2014), and Zheng *et al.* (2015) all showed the presence of large summer rainfall centres in the northeast mountainous areas and near the urban area, respectively. Yang *et al.* (2013) also mentioned that heavy rainfall events contributed much to total rainfall amount, especially at the nighttime. After analysing the frequency of heavy rainfall, Cao *et al.* (2016) found that the urban area and the northeastern region of Beijing experienced frequently short-duration heavy rainfall events with the accumulated precipitation of over 50 mm. The above studies all used hourly rainfall data from the BMR's AWSs, but few of them focused on the statistical characteristics of HHR events. Therefore, we are motivated to fill this gap by examining the statistical characteristics of HHR events over the BMR.

A few statistical studies of heavy rainfall events have been carried out in some geographical regions. Brooks and Stensrud (2000) analysed the climatology of heavy rainfall events in the United States in order to better understand the threat of flash floods. They found a seasonal cycle in the distribution of heavy rainfall events beginning along the Gulf Coast and expanding into the midwestern states during the summer season. Chen *et al.* (2007) found that heavy rainfall days, which were not related to typhoon, were frequent from mid-May to early October in Taiwan and the distribution of the associated heavy rainfall events was affected by local topography and low-level winds. Zhang and Zhai (2011) examined the spatiotemporal characteristics of hourly extreme rainfall in the warm season in China, based on hourly precipitation data from 575 stations, and pointed out that extreme rainfall events over Northern China are most frequent in late afternoon and early evening. Chen *et al.* (2013) investigated the warm-season short-duration heavy rainfall in China using hourly rain gauge data from 876 stations, and also found that the heavy rainfall over North China peaks in the afternoon and near midnight. Iwasaki (2012, 2015) found significant positive heavy rainfall trends from June to September in eastern Japan, which were closely related to the variation of lower-tropospheric moisture fluxes.

A statistical analysis of HHR events over the BMR could not be possible until 2005 when a dense AWSs operational network began to set up, and one year later its expansion was completed in preparing for the opening of the Beijing – 2008 Olympic Games (Dou *et al.*, 2008). Data quality control at daily basis and evaluation of the AWSs observations have also been performed, showing satisfactory accuracy and reliability (Dou *et al.*, 2008; Yang and Liu 2013). After more than 8-years successful operations, it is now feasible to conduct a statistical analysis of HHR events over the BMR using all the available AWS observations with high spatial and temporal resolutions. It should be mentioned that such a high-resolution data has not been fully used by the previous studies mentioned above.

The objectives of this study are to (1) examine the spatial and temporal characteristics of HHR events over the BMR, (2) document the occurrences of extreme HHR events in terms of location, frequency, rainfall amount and intensity as well as duration and area coverage, and (3) identify the likely key local factors that may influence the occurrences of extreme and more frequent HHR events for the given climatological conditions during the warm seasons over the BMR. The above objectives will be achieved by analysing the AWS's observations at 5-min intervals during the warm seasons of 2007–2014.

The next section describes the data source and methodology used for this study. Sections 3–5 present the spatial distributions, semi-monthly and diurnal characteristics of HHR events, respectively. Extreme and more frequent HHR events over the BMR will be also documented. Section 6 shows an analysis of the averaged surface meteorological fields obtained from the AWS network and the averaged upper-air conditions over the BMR on HHR and non-HHR days, and then discusses their possible influences on the occurrences of some HHR events. A summary and conclusions are given in the final section.

## 2. Data source and methodology

In this study, observational data at 5-min intervals from the 155 AWSs over the BMR during the 8-years period (2007–2014), archived at the Beijing Meteorological Bureau, are used (see Figure 1). This dataset, prior to its usage, has gone through data quality control by checking for extreme rainfall values and temporal continuity, following Dou *et al.* (2008). Rainfall records exceeding 40 mm in 5 min were removed; when hourly rainfall, after adding up every 12 consecutive 5-min rainfall records, exceeds 145 mm, the relevant 5-min records were not used (Ren *et al.*, 2010, 2015); and stations with missing data over 5% of the total records during the 8 years were eliminated. The 155 AWSs have also undergone similar screening processes in order to analyse other meteorological variables, which yielded 153, 95 and 137 stations for acceptable surface temperature, specific humidity, and horizontal winds, respectively.

Since this study is concerned with HHR events during warm seasons, we define an HHR event as an hourly rainfall amount greater than 20 mm, following the definition of short-duration heavy rainfall events by the China Meteorological Administration (CMA). The 20 mm $h^{-1}$ rate has been demonstrated by Zhang and Zhai (2011) to be a reasonable criterion to study short-duration heavy rainfall events in China. Selected HHR events have also been verified against satellite and radar data.

Following the methodology adopted by Wang and Wang (2013), an HHR event is assumed to begin at the time when

 

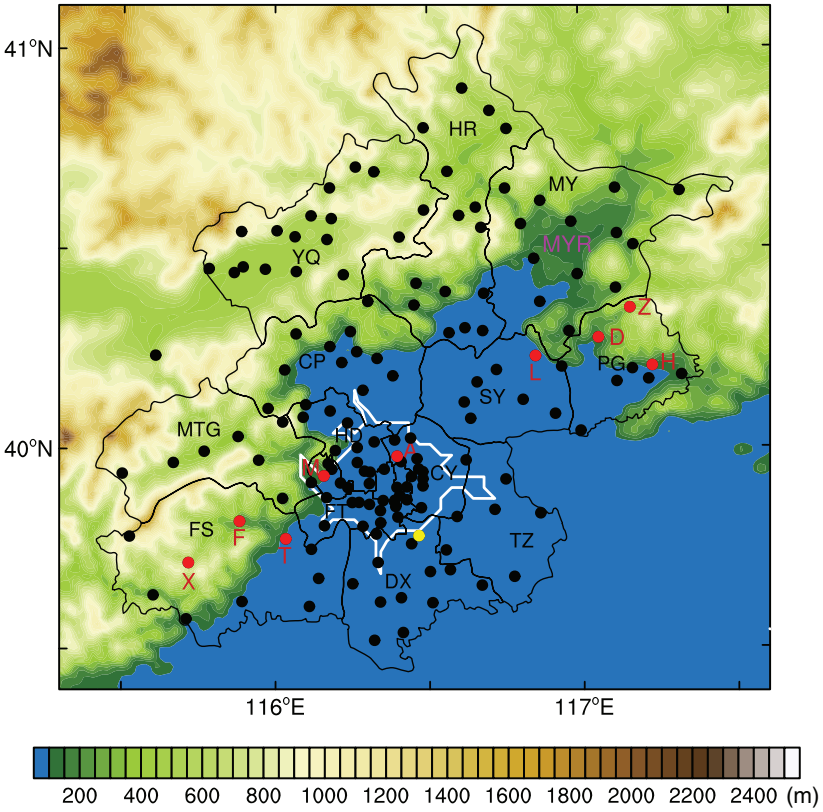


Figure 1. Distribution of the 155 AWS stations (dots) used for this study, superimposed with terrain (shaded, m). Beijing's district names are abbreviated in an alphabetic order as follows: CP (Changping) CY (Chaoyang), DX (Daxing), FS (Fangshan), FT (Fengtai), HD (Haidian), HR (Huairou), MTG (Mentougou), MY (Miyun), PG (Pinggu), SY (Shunyi), TZ (Tongzhou) and YQ (Yanqing); the two small Eastern and Western Districts, located to HD's immediate southeast, and Shijingshan District to HD's immediate southwest, are not denoted. MYR denotes the location of the Miyun Reservoir. Similarly for the rest of figures. Red dots, and letters, 'H' (Heidouyu, PG), 'A' (Aotizhongxin, CY), 'D' (Dahuashan, PG), 'X' (Xiayunling, FS), 'M' (Moshikou, Shijingshan), 'F' (Fozizhuang, FS) and 'T' (Tuoli, FS), denote the locations of stations at which certain extreme events occurred (see Table 1). 'Z' (Zhenluoying, PG) and 'L' (Longwantun, SY) denote the locations of the two stations mentioned in Section 3. Yellow dot denotes the location of Beijing observatory. Urban and built-up areas in the MODIS land use categories near the central districts are delineated with white contours.

Table 1. A list of the stations (see Figure 1 for their locations) at which one of the following extreme HHR events during the warm seasons of 2007–2014, as bolded, was recorded: the total frequency of HHR events (FRQ) and the corresponding total rainfall amount ($RN_{TT}$, mm); the starting time (Year-Month-Date-LST), duration (hours), and the accumulated rainfall ($RN_{AC}$, mm) associated with a single HHR event, the maximum rainfall intensity in an hour ($RI_{1H}$, mm $h^{-1}$) and in 5 min [$RI_{5M}$, mm (5 min)$^{-1}$].

| Station | FRQ | $RN_{TT}$ | Starting time | Duration | $RN_{AC}$ | $RI_{1H}$ | $RI_{5M}$ |
|---|---|---|---|---|---|---|---|
| Heidouyu[2] | **40** | 1274.9 | 12-07-21-2010 | 4.17 | 162.7 | 76.5 | 12.1 |
| Aotizhongxin[1] | 37 | **1517.9** | 12-07-21-1710 | 5.17 | 133.7 | 63.8 | 9.8 |
| Dahuashan[2] | 31 | 1254.9 | 12-07-21-1500 | **8.75** | 228.6 | 94.4 | 15.2 |
| Xiayunling | 20 | 857.6 | 12-07-21-1030 | 8.5 | **281.5** | 81.4 | 11.8 |
| Moshikou | 26 | 1054.7 | 11-06-23-1600 | 2.75 | 180.3 | **135.7** | 23.9 |
| Fozizhuang | 15 | 771.7 | 08-06-13-1900 | 1 | 129.2 | 129.2 | **32.4** |
| Tuoli | 29 | 1240.9 | 12-07-21-1615 | 5.75 | 255.3 | 103.6 | 12.2 |

Another extreme HHR event associated with the 7–21 extreme rainfall event is also listed in the bottom row. Superscript in the first column denotes the region of high-frequency HHR events: '1' for the central urban districts, and '2' for the northeast mountains; and otherwise not in any high-frequency HHR event region.

more than or equal to 0.1 mm rainfall is accumulated in the next 5 min and more than or equal to 20 mm in 1 h. Then, the accumulated rainfall amount for an HHR event is calculated every 5 min until the time when less than or equal to 5 mm rainfall is recorded in the next 1 h, and this time is considered as the ending time of the HHR event. The duration of the HHR event is defined as the minutes between the starting and ending time.

Note that with the above procedures the duration of an HHR event could last for more than an hour. In fact, Table 1 shows that (1) the longest duration of an HHR event, recorded at the Dahuashan station in Pinggu starting from 1500 LST (LST = UTC + 8) 21 July 2012, was 8.75 h, with an accumulated rainfall amount of 228.6 mm, and (2) the most extreme rainfall amount accumulated in an HHR event, recorded at the Xiayunling station in Fangshan

 

starting from 1030 LST 21 July 2012, was 281.5 mm in 8.5 h. Note also that the long duration of an HHR event could be caused by the passage of several mesoscale convective systems (MCSs) in sequence as long as the hourly rainfall following the previous HHR-producing system was more than 5 mm. This was true for the 8.75 h duration obtained in association with the 7–21 extreme rainfall event in which three different types of HHR-producing MCSs passed by the BMR (see Zhang *et al.* 2013; Zhong *et al.* 2015).

It is evident that the above procedures for determining the ending time and duration help detect those HHR events with accumulated rainfall reaching 20 mm in less than 1 h. Previous studies using rainfall data at hourly intervals may discretize hourly accumulated rainfall amount exceeding 20 mm associated with one complete HHR event into two hourly intervals, thus failing to identify it as an HHR event. This problem will not appear in the analyzes using the rainfall observations at 5-min intervals in the present study.

## 3. Spatial distributions of HHR events

Figure 2(a) and (b) shows the spatial distributions of the total frequency (or number) of HHR events and the corresponding rainfall amounts, respectively. We see significant variability in the HHR frequency and associated rainfall amount across the BMR, with nearly an order of magnitude difference from the southeastern to northwestern boundary. High-frequency HHR events were located in eastern Haidian, and around the northeast mountains in Shunyi, Miyun and Pinggu where prevailing southerly flows of moist air were often uplifted during the warm seasons, as will be shown in Section 6. The Heidouyu station in Pinggu recorded the most frequent HHR events of 40 during the 8-years warm seasons (see Table 1), and then 38 HHR events at the Zhenluoying station in Pinggu. The generation of the high-frequency HHR events in eastern Haidian and northeast mountains indicates the likely roles of urban effect and topography (Figure 1), respectively, in favouring the generation of local HHR events. In contrast, low-frequency HHR events could be seen in the west mountains of Mentougou, and the northwest mountains of Yanqing and Huairou. The HHR frequency differences between the Haidian and its west mountainous region are as large as more than 25 events in less than 25 km (Figure 2(a)).

Overall, the median frequency of HHR events was 24 over the BMR, and 90% of the 155 stations recorded a total of 7–36 HHR events during the 8-years warm seasons, as shown by a box and whisker plot in Figure 3(a). The 155 stations were ranked in Figure 3(b), based on the total frequency of HHR events during the 8-years period, showing that a large portion of the stations ranked in the lowest quartile, i.e. less than 18 events, were situated over the west and northwest mountains. By comparison, the stations ranked in the top quartile, i.e. greater than 29 events, were located in the BMR's central urban districts, and near the northeast mountainous regions in Shunyi, Miyun and Pinggu. The results emphasize again that urban effect and local topography are probably the two important factors in determining the occurrences of HHR events in the BMR, given favourable large-scale conditions during the warm seasons.

Like the HHR frequency, the total rainfall distribution of the HHR events also shows large rainfall centres in eastern Haidian, and around the northeast mountains in Shunyi, Miyun and Pinggu (Figure 2(b)). The Aotizhongxin station in Chaoyang observed a total rainfall amount of 1517.9 mm from HHR events during the 8-years warm seasons (see Table 1). The Zhenluoying station in Pinggu and the Longwantun station in Shunyi observed a total rainfall amount of more than 1400 mm. By comparison, most of the west and northwest mountainous regions recorded very small rainfall amount (not shown). For the 8-years warm seasons, much less than 500 mm total rainfall associated with the HHR events was produced (Figure 2(b)).

Some extreme HHR events brought record-breaking rainfall. The maximum hourly rainfall rate is 135.7 mm $h^1$ recorded at the Moshikou station in Shjingshan on 23 June 2011, and the extreme rainfall in 5 min is 32.4 mm recorded at the Fozizhuang station in Fangshan on 13 June 2008 (see Table 1). During the 7–21 extreme rainfall event, 124 AWSs spreading over all the BMR's districts observed HHR events, in which Xiayunling and Tuoli in Fangshan recorded a total rainfall amount of 281.5 mm in 8.5 h, and 103.6 mm in an hour (see Table 1), respectively. Since the 7–21 extreme rainfall event was so heavy, we have compared the spatial distributions of frequency and rainfall amounts of the HHR events with and without the 7–21 event in order to see if it would influence our statistical results. Results show little impact on the general characteristics of the statistical results, including large and small-valued centres, but do show reduced rainfall amounts (not shown).

Rainstorm days, defined by the CMA as a daily rainfall amount of more than 50 mm, has also been used in China as a measure of heavy rainfall for issuing flash flooding warning. With this definition, a rainstorm day may be caused by either short-duration heavy rainfall events or light rainfall events with long durations. Because of this similarity and difference between an HHR event and a rainstorm day, both the frequency and rainfall amount of rainstorm days should be examined separately, and their spatial distributions are given in Figure 2(c) and (d), respectively. (A daily rainfall amount is obtained by adding up the rainfall amount from 0800 LST to 0800 LST on the next day.) Like the HHR events, the frequency of rainstorm days was low in the west and northwest mountains while high-frequency rainstorm days were generally centred over the eastern portion of Hadian and the southeast plains of Daxing (Figure 2(c)). Secondary centres could also be seen in Miyun and Pinggu. However, the peak frequency of rainstorm days (i.e. in Daxing) differed from that of the HHR events (i.e. in Pinggu) (cf. Figure 2(a) and (c)). On the other hand, the distribution of the total rainfall amounts on rainstorm days is more similar in pattern to that associated with the HHR

 

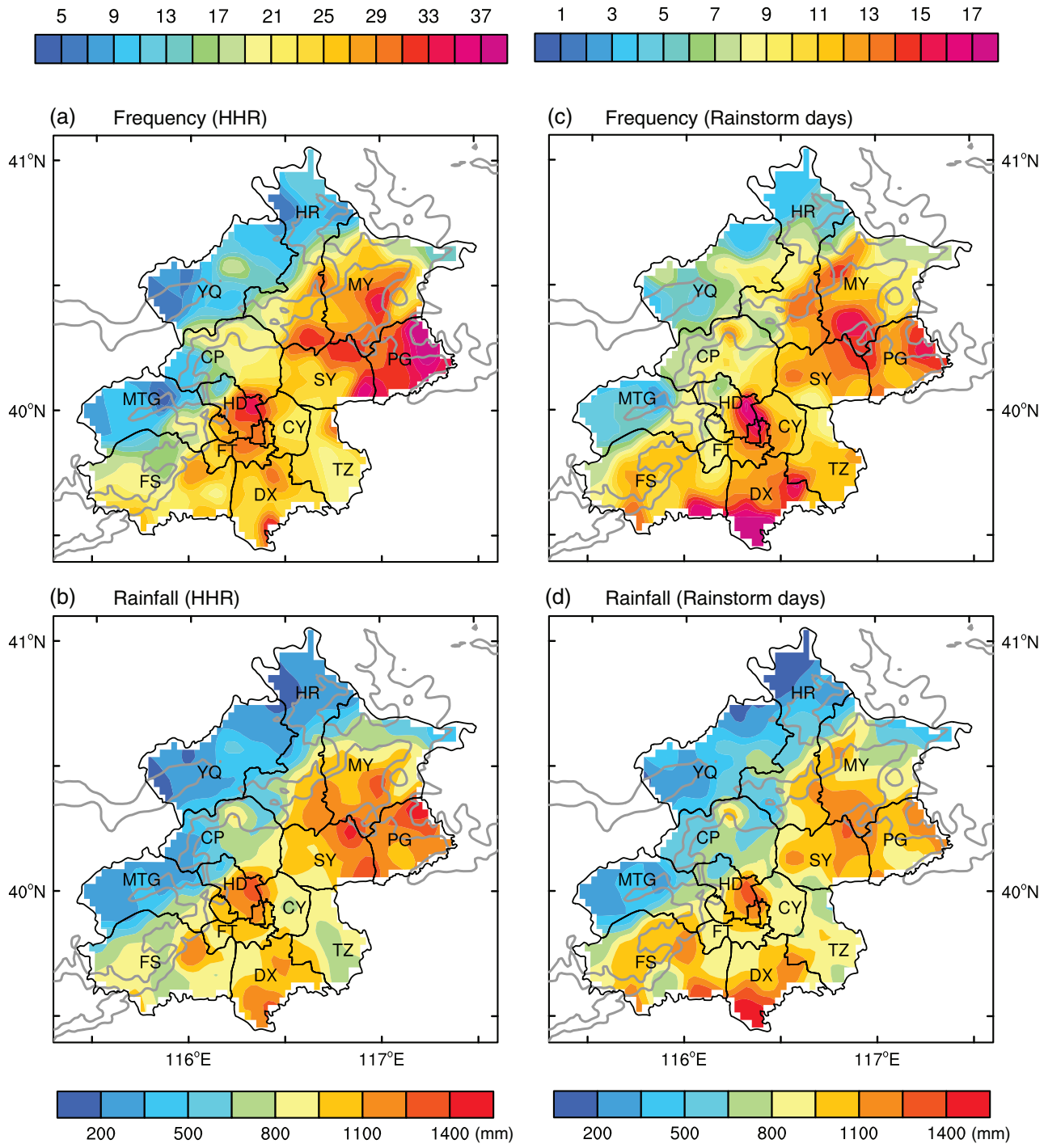


Figure 2. The total frequency (or number) of (a) HHR events (shaded), and (b) the corresponding rainfall amounts (shaded, mm) during the warm seasons of 2007–2014. (c) and (d) As in (a) and (b), respectively, except for rainstorm days (shaded). Grey solid lines are isohypses of 200 m and 500 m; similarly for the rest of figures.

events than that of the total frequency (cf. Figure 2(b) and (d)).

To see how significant the HHR events and rainstorm days were in accounting for local warm-seasonal rainfall over the BMR, Figure 4(a)–(c) shows the total rainfall amounts, including those from both the HHR and non-HHR events, and the percentage contributions from the HHR events and rainstorm days, respectively. The most prominent feature was the peak rainfall of more than 4400 mm near the northeast mountains in Pinggu, which coincided with those of high-frequency HHR events (Figures 4(a) and 2(a)). A secondary large rainfall centre in the range of 4200–4400 mm could be seen in the northeast of Shunyi. Other large rainfall centres in the range of 4000–4200 mm could be seen over the BMR's central urban districts, southern Daxing, and the central western Fangshan (Figure 4(a)). The total rainfall amount was mostly less than 3000 mm in the west and

 

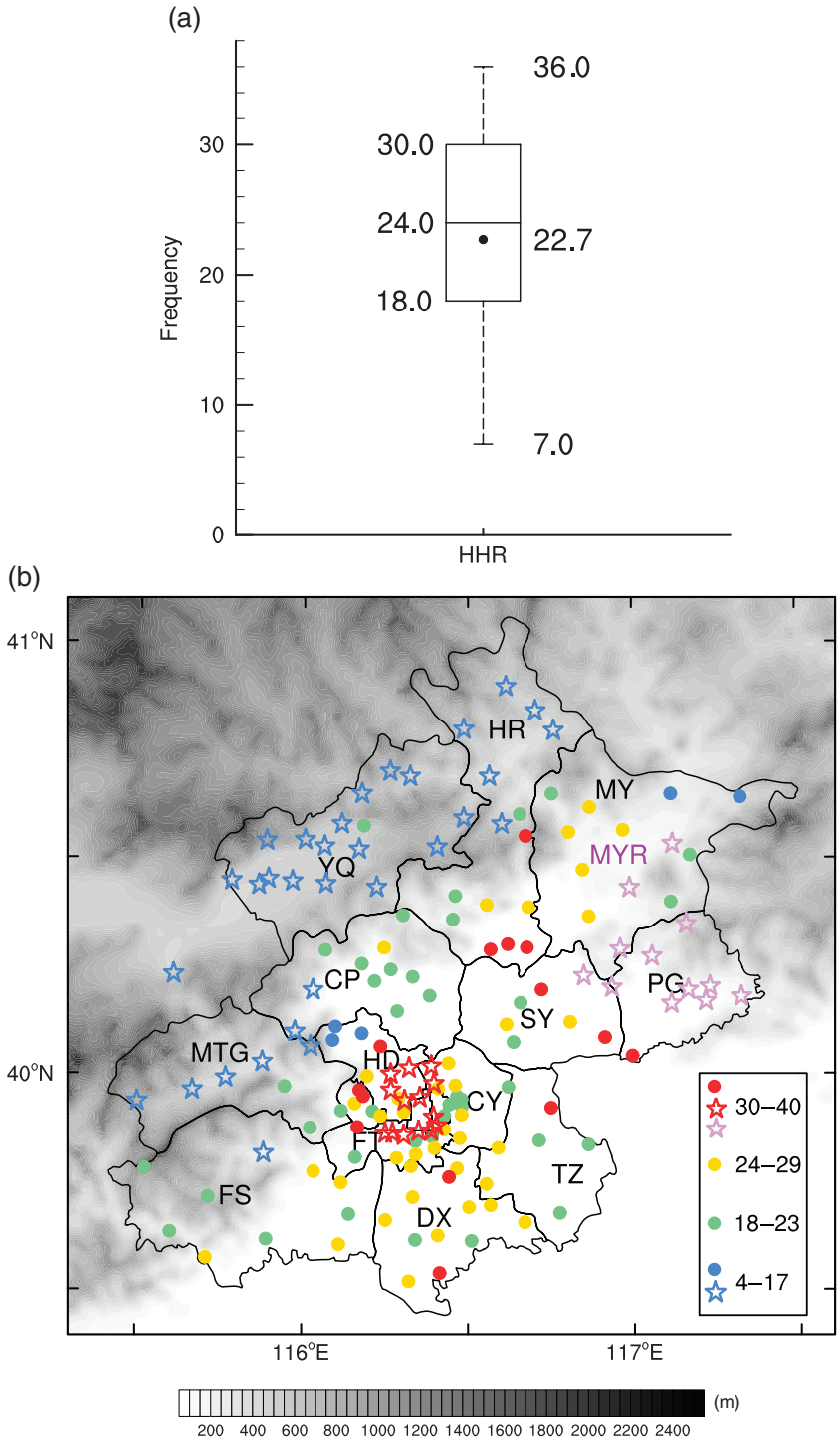


Figure 3. (a) Box and whisker plot of the total frequency of HHR events during the warm seasons of 2007–2014 recorded by each AWS. The box shows the interquartile range. The horizontal line and dot in the box indicate the median and mean value, respectively. The bottom and top short lines denote the 5th and 95th percentiles, respectively. (b) Distribution of four different ranks of AWSs, as classified according to their total frequencies of HHR events: 30–40 events marked by red dots, and red stars for the central urban districts and plum stars for the northeast mountains, 24–29 events marked by orange dots, 18-23 events marked by green dots, and 4–17 events marked by blue dots or blue stars. The star marks in three different colours denote the three different representative AWSs used in Figures 7 and 8(b), and discussed in Sections 4 and 5. The background grey shadings show terrain elevations (m).

northwest mountains with the terrain elevations of over 500 m. The distribution of warm-seasonal rainfall amount (Figure 4(a)) is similar to that of summer rainfall presented in Yang *et al.* (2013), Liu *et al.* (2014), and Zheng *et al.* (2015).

Figure 4(b) and (c) reveals that both the HHR events and rainstorm days in the west and northwest mountains made small contributions to the local total warm-seasonal rainfall, mostly less than 15%. The HHR events contributed more than 30% to the total warm-seasonal rainfall in

 

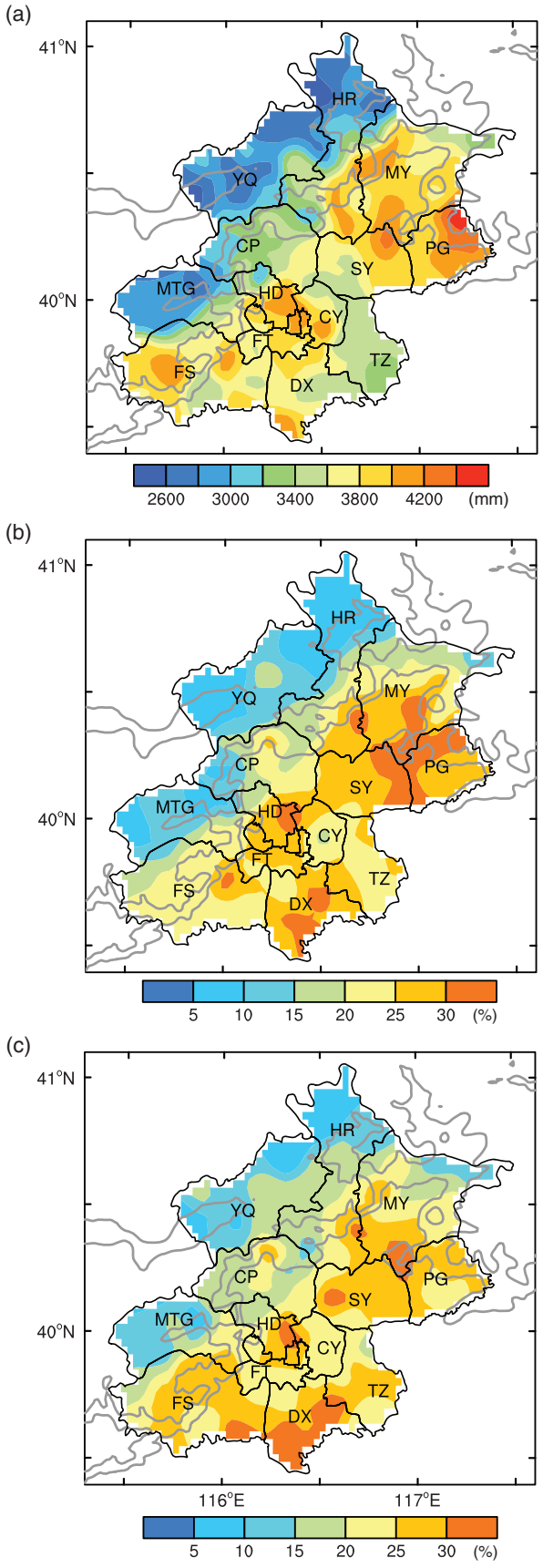


Figure 4. (a) Total rainfall amounts (shaded, mm) from those including both HHR and non-HHR events during the warm seasons of 2007–2014. Relative contributions (shaded, %) of rainfall amounts from (b) HHR events and (c) rainstorm days to the total rainfall amounts.

Miyun, Pinggu and Shunyi, in eastern Haidian, and southern Daxing. The rainstorm days exhibited more than 30% relative contributions over the southeastern half portion of Daxing, and near the Miyun-Pinggu-Shunyi border and eastern Haidian. Thus, the frequencies of HHR events and rainstorm days were consistent with each other in accounting for a sizeable amount of total rainfall in Miyun, Daxing, and eastern Haidian.

Catastrophic disasters are more likely to occur on the rainstorm days with HHR events than on the rainstorm days resulting from light rainfall but with long duration. Thus, it is necessary to examine the proportion of rainstorm days on which HHR events occurred. For this purpose, Figure 5 shows the proportion of rainstorm days with HHR events at each station in the form of a pie graph, with the corresponding frequency shown by the pie's colour. Clearly, the rainstorm days with HHR events accounted for more than 50% of the total rainstorm days at almost all the stations over the plains and around the northeast mountains, where are also the regions of high-frequency rainstorm days. At the stations in the northwest mountains in Yanqing and Huairou, not only fewer rainstorm days were recorded but also the proportions of the rainstorm days with HHR events were small. Few rainstorm days with HHR events were observed at five stations located over the western mountainous regions, each of which only recorded fewer than 4 rainstorm days during the 8-years warm seasons.

Rainfall intensity is an important parameter in influencing the rainfall statistics and the degree of disasters caused during the passage of a thunderstorm. Limited by the temporal resolution of observations, previous studies have usually estimated rainfall intensity at most with an hourly resolution. However, some short-term torrential rain may last for about 1 h or less. Since we have obtained the 5-min rainfall dataset, it would be of interest to examine the statistics of rainfall intensity with such a high temporal resolution data.

A box and whisker plot, given in Figure 6(a), shows that the median rainfall intensity for all the HHR events was 2.6 mm $(5\,\text{min})^{-1}$ and that about 90% of the HHR events ranged between 1.5 and 6.2 mm $(5\,\text{min})^{-1}$. The spatial distribution of the 5-min median rainfall intensity shows quite different patterns from that of the HHR frequency and associated rainfall amount (Figures 6(b) and 2(a) and (c)). That is, high (5-min) intensity centres appeared in the low-HHR frequency regions in Yanqing and Huairou, whereas the high-HHR frequency regions in Miyun, Pingu and Haidian had relatively lower (5-min) rainfall intensity. This implies that the former two regions might have experienced the passage of intense rain-producing thunderstorms or shorter- (than an hour) lived heavy-rain-producing systems. Of course, the relatively small sample size in these regions might also impact the rainfall statistic result. The results indicate that the HHR events over the latter regions were associated mostly with thunderstorms producing weaker- (5 min) intensity rainfall. On the other hand, the median intensity centre near the Pinggu-Shunyi border was

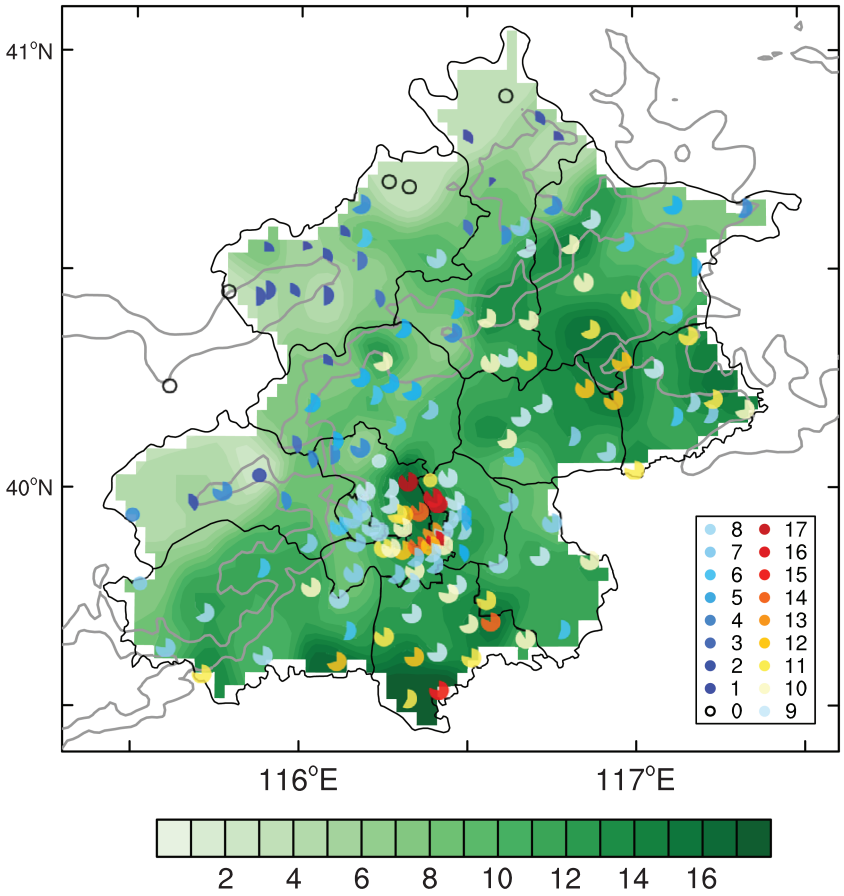


Figure 5. The pie chart at each station represents the proportion of rainstorm days with the occurrences of HHR events and the pie colour depicts the total number of these rainstorm days as shown in the legend. A hollow circle indicates a null value. The background green shadings denote the total frequency of rainstorm days as shown in Figure 2(c).

more or less consistent with that of relatively higher-HHR frequencies.

## 4. Semi-monthly variation of HHR events

Figure 7 shows the semi-monthly variation of the mean frequency and the mean rainfall amount of HHR events over the BMR during the warm seasons. The general features shown in Figure 7(a) and (b) are similar. Only a few HHR events occurred in May, so the corresponding total rainfall amount is small. Both the frequency and rainfall amount increased sharply from the early June, and then peaked in late July when the strongest solar energy is received. A dramatic increase in rainfall amount occurred from early to late July. Liu *et al.* (2014) also noted the BMR's peak of total rainfall amount occurring in July. The HHR frequency became significantly lower in late August, and so was the rainfall amount. A similar trend but different magnitudes appeared in the frequency of rainstorm days. The peak frequency of the rainstorm days is lower than that of the HHR events in the late July, but the peak rainfall amount of the rainstorm days is greater than that of the HHR events, which could be partly attributed to the occurrences of more than one HHR event in one day.

Given the large variability in HHR events between the BMR's mountainous regions and central urban districts, we examine the semi-monthly variations for the following three different groups of representative stations, as indicated by stars marked in Figure 3(b): low-frequency HHR stations in the west and northwest mountains, high-frequency HHR stations in the central urban districts, and high-frequency HHR stations near the northeast mountains. They are also plotted in Figure 7, showing that the frequency and rainfall amount of HHR events at the low-frequency stations over the west and northwest mountains was near-uniformly distributed from the early June to early August.

The semi-monthly variations at the high-frequency stations over both the central urban districts and the northeast mountains resembled those at all the stations, i.e. peaking in late July. The increased HHR frequency over the former region occurred more sharply from early to late July than that over the latter region, whereas the rainfall amount of the HHR events increased dramatically over both regions. The rising trend from late June to late July, and falling trend from late July to early September, correspond well to the periods of northward-advancing and southward-retreating monsoonal flows, respectively. Distinctly more HHR events near the northeast mountains than

 

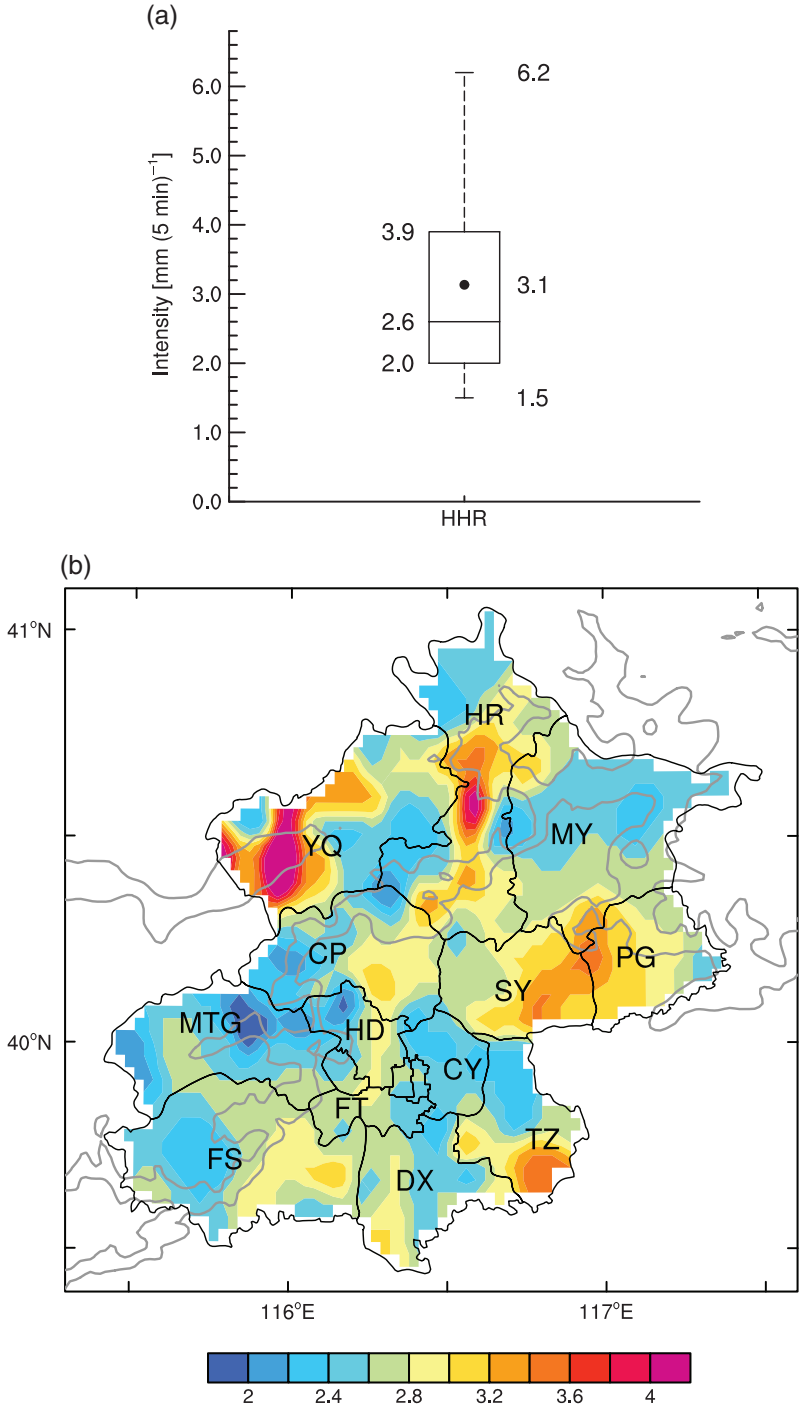


Figure 6. (a) As in Figure 3(a) but for rainfall intensity [mm (5 min)$^{-1}$] of all the HHR events during the warm seasons of 2007–2014. (b) Spatial distribution of the median rainfall intensity [shaded, mm (5 min)$^{-1}$] of HHR events.

those in the central urban districts occurred in late June, early July, late August and late September, indicating again the topographical lifting effects on the generation of HHR events over the BMR's northeastern region.

## 5. Diurnal variation of HHR events

After seeing the semi-monthly variation of HHR events, it is of interest to examine during which period of a day the HHR events were more likely to start over the BMR. For the convenience of data processing, we divide a diurnal cycle into the following four periods: before dawn (0000–0559 LST), morning hours (0600–1159 LST), afternoon hours (1200–1759 LST), and evening hours (1800–2359 LST). For each station, the most frequent starting period of HHR events is denoted in Figure 8(a) by an arrow. Note that only those stations with over 40% of the total HHR events starting in the most frequent starting period are plotted with arrows. Apparently, HHR events started frequently in the afternoon hours at most stations

 

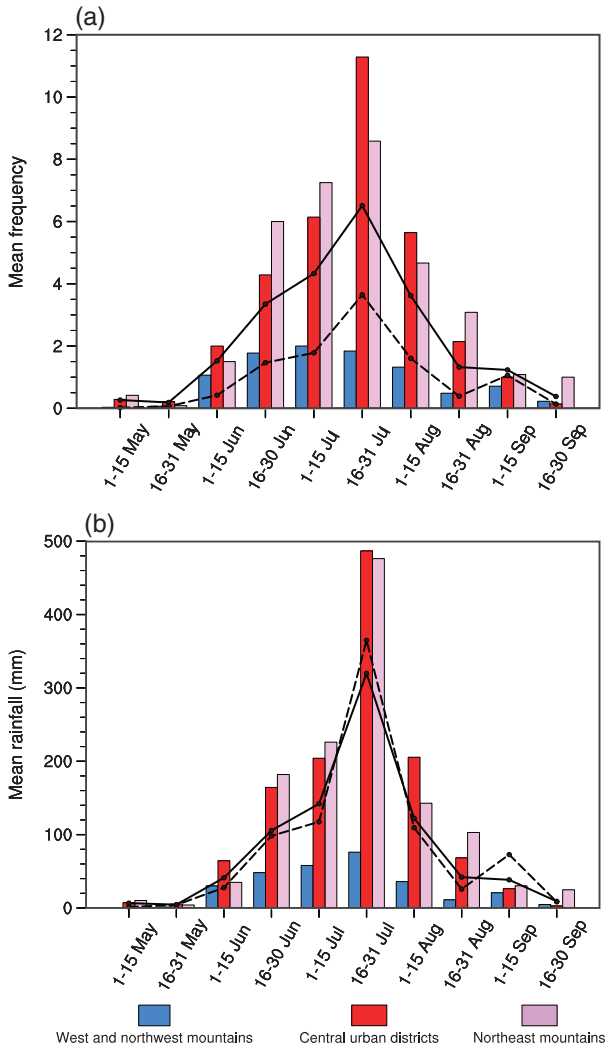


Figure 7. Semi-monthly variation of (a) the mean frequency and (b) mean rainfall amount of HHR events (solid line) and rainstorm days (dashed lines) per station for all the 155 stations over the BMR during the warm seasons of 2007–2014. The bar charts display the mean frequency and mean rainfall amount of HHR events per station in three representative groups: blue for the west and northwest mountains; red for the central urban districts; and plum for the northeast mountains. These representative stations are denoted by stars marked in Figure 3(b) in the same colours. The mean value is obtained by averaging the frequencies or rainfall amounts at all the stations in the same group.

in Mentougou and Yanqing, i.e. over the west mountainous regions, and in the evening hours at stations in most of the other districts. We may speculate that some HHR events were likely initiated over the west mountains in the afternoon hours when surface heating is peaked with prevailing south- to southeasterly flows to be shown in Section 6, and then the associated thunderstorms propagated eastward into the plain regions. Little dominant signals of the HHR-starting times could be seen in the central urban districts, Tongzhou, and southwestern Fangshan, implying that HHR events over the regions occurred during any periods.

The diurnal variations of the total frequency of HHR events, plotted at their starting times, are given as a solid line in Figure 8(b), showing that the total HHR frequency was less than 90 over the BMR from 0400 to 1200 LST, and it increased sharply after 1300 LST and reached a frequency of more than 250 at 1600 LST, and then the peak frequency of nearly 300 at 1900 LST with a slight drop between 1600 and 1900 LST. These peak periods agree with the finding of Zhang and Zhai (2011) and Chen *et al.* (2013). The total frequency of the HHR events decreased after 2000 LST, but it was still pronounced (i.e. more than 150) even shortly after midnight.

The above variations are different when the three different representative regions (dashed lines in different colours), as mentioned before, are considered. At the high-frequency stations in the central urban districts (red dashed), on average HHR events were less likely to start during the morning hours, though with a small peak at 0800 LST. More active HHR events occurred during the late afternoon and early evening hours. Similarly for stations in the northeast mountains (plum dashed line), except for the much less pronounced fluctuations. The more pronounced fluctuations of HHR events for the central urban districts appear to be attributable to the use of a too small area coverage across which thunderstorms with HHR moved (see Figure 3(b)). The diurnal variation of low-frequency HHR events at stations in the west and northwest mountains (blue dashed) was much smoother than the other two representative groups, with an active period from 1400 to 0000 LST and a peak at 1600 LST.

## 6. Possible influences of regional surface and upper-air conditions

Clearly, the generation of HHR events results from multi-scale interactions ranging from cloud microphysical and convective processes to mesoscale organization, frontal and larger-scale forcing (Houze *et al.*, 1989; Chen *et al.*, 1991; Chen and Li, 1995; Houze, 2004; Iwasaki, 2012, 2015; Zhang *et al.*, 2013; Zhong *et al.*, 2015). This is especially true for those long-lasting HHR events, in which continued boundary-layer forcing and large-scale moisture supply, and some favourable mesoscale processes such as the echo and band trainings (Doswell *et al.*, 1996; Luo *et al.*, 2014), would play important roles. Statistical studies by Wilson *et al.* (2007) and Chen *et al.* (2014) indicated that cold vortices and westerly midlevel troughs are the main synoptic weather systems influencing the occurrence of convective storms over the BMR during the warm season, and subtropical high is another important system.

On the other hand, our analyzes in the preceding sections indicate some correlations between HHR events and surface conditions (e.g. topography, urban environment). This suggests that certain surface conditions might have provided some positive influences on the generation of the HHR events. Thus, it is desirable to analyse the surface temperature, humidity, and horizontal winds at all the AWSs and then discuss to what extent the HHR events were closely related to some surface meteorological conditions. For this reason, the surface conditions on HHR days

 

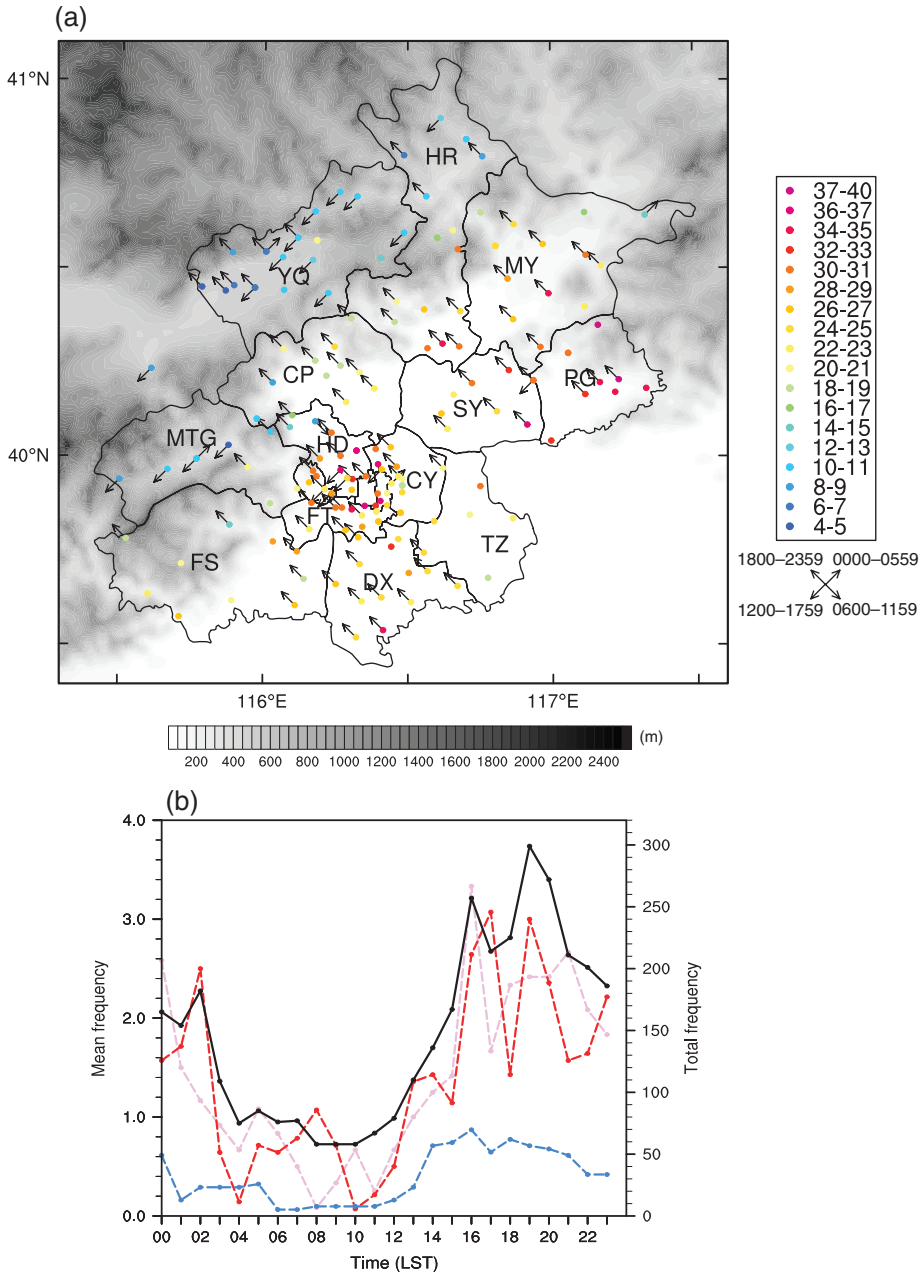


Figure 8. (a) The most frequent starting period of HHR events at each station (dotted), as represented by an arrow direction given in the right bottom corner. The arrows pointing to the northeast, southeast, southwest, and northwest denote the periods of 0000–0559, 0600–1159, 1200–1759 and 1800–2359 LST, respectively. Only those stations with over 40% of the total HHR events occurring in the most frequent starting period are drawn with arrows. The dot colour denotes the total frequency of HHR events at each station as shown in the right legend. The background grey shadings show terrain elevations (m). (b) Diurnal variation of the total frequency of HHR events over the BMR (solid line), and the mean frequency of HHR events at the three representative groups of stations (over the west and northwest mountains by blue-dashed lines; the central urban districts by red-dashed lines; and the northeast mountains by plum-dashed lines) during the warm seasons of 2007–2014. The mean frequency per station is calculated in the same way as that in Figure 7. The right (left) y-axis applies to the solid line (dashed lines).

and non-HHR days are analysed separately to find their similarities and differences. Here a HHR day (0800–0800 LST) is selected when at least five stations recorded HHR events, while a non-HHR day is designated when no station recorded any HHR events. Applying this procedure results in 149 HHR days and 863 non-HHR days. Figures 9 and 10 present the averaged surface temperature and specific humidity fields superimposed with surface streamlines, respectively, at 0800 and 1400 LST on the HHR days and non-HHR days. The two time levels are selected, respectively, because of the designated starting time of a HHR (non-HHR) day and the occurrences of the peak frequency of late-afternoon HHR events as shown in Figure 8. We should mention that the BMR during the warm season is typically dominated by southerly winds in the lower troposphere over the plain region, which is modulated by mountain-plain circulations (Miao *et al.*, 2009) and inertial oscillation (Blackadar 1957; Zhang and Zheng 2004).

 

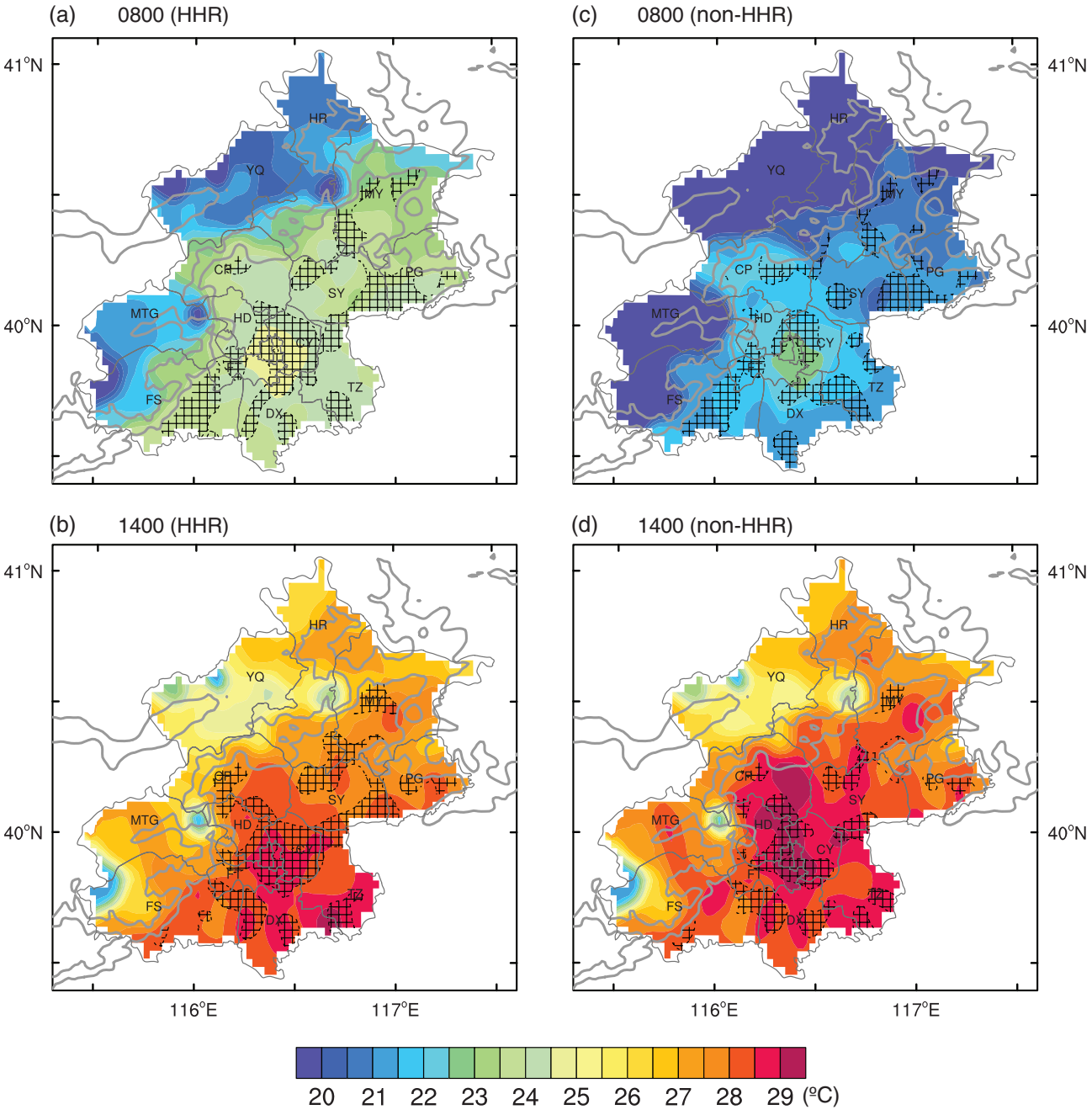


Figure 9. Distribution of the temporally averaged surface temperature (shaded, °C), and convergence zones (hatched zones depicting the zones with divergence values $\leq -10^{-5}$ s$^{-1}$; no calculations made for the mountainous areas higher than 200 m), observed by the AWSs at (a) and (c) 0800 LST; (b) and (d) 1400 LST on HHR days (left), and non-HHR days (right) during the warm seasons of 2007–2014.

This can also be seen from the averaged surface streamlines given in Figure 10, showing dominant southerly flows during the daytime and some evidence of downslope winds from the west and northeast mountains during the nighttime. In addition, the central urban districts were distinctly warmer, with more organized convergence, than any other region (Figure 9), which is clearly a typical urban heat island effect (Zhang *et al.*, 2009).

Of more relevance to this study is that surface temperature and moisture at 0800 LST on HHR days were, respectively, warmer and higher than those on non-HHR days. These conditions were consistent with the colder and drier northerly flows and downslope winds on non-HHR days compared to more easterly flows over the plain regions and much less coverage of downslope winds over the mountainous regions on HHR days (Figures 9(a) and (c) and 10(a) and (c)). Although the surface temperature field at 1400 LST exhibited little differences, one can see (about 3–4 g kg$^{-1}$) higher specific humidity on HHR days, especially over the Changping-Haidian-Chaoyang borders, Daxing and Shunyi districts which coincided roughly with more HHR events and rainfall amounts (cf. Figures 10(b) and (d) and 2(a) and (b)). Clearly, a moist boundary layer tends to be more conditional unstable for

 

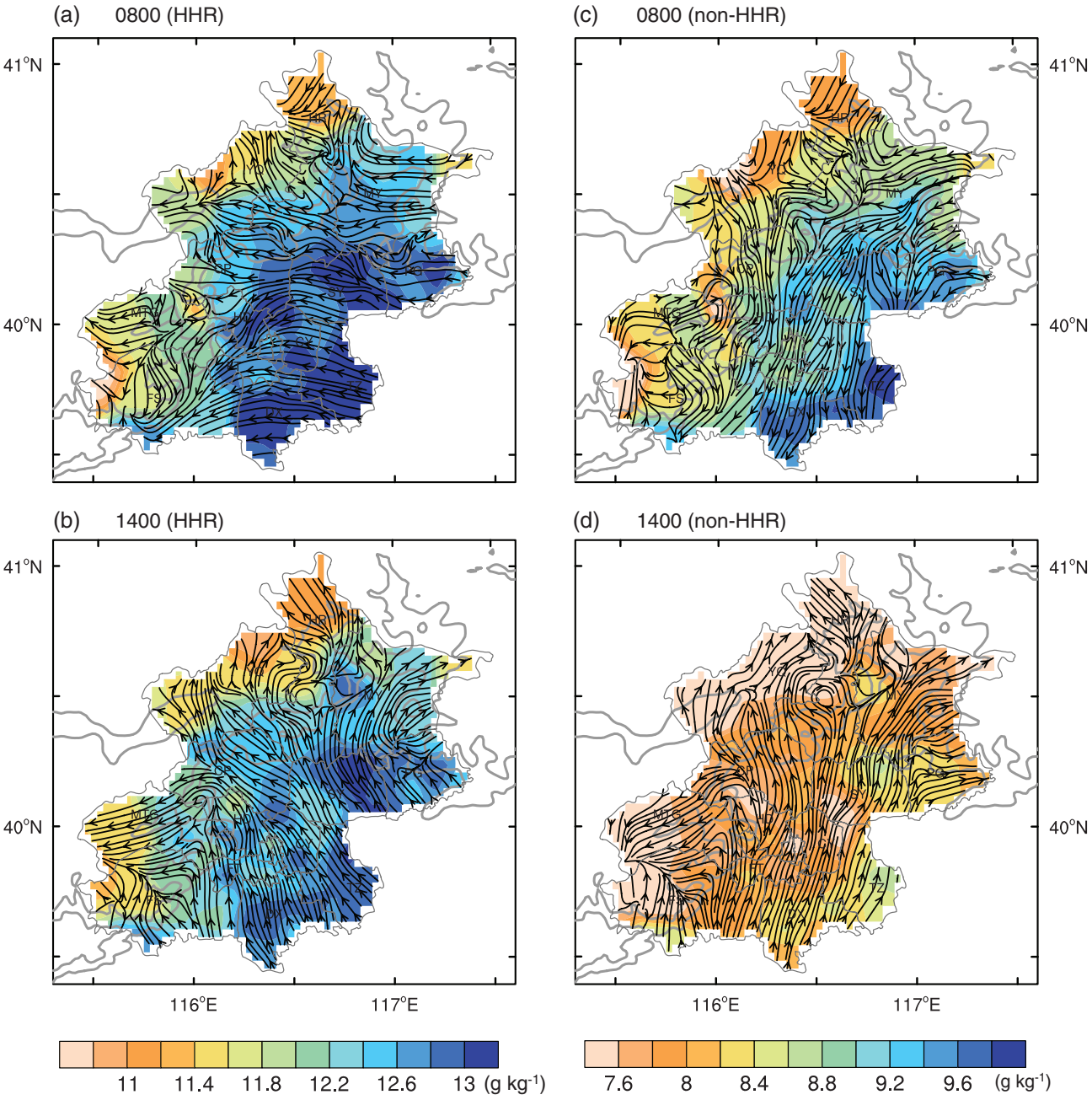


Figure 10. Distribution of the temporally averaged specific humidity (shaded, g kg$^{-1}$), superimposed by surface streamlines, observed by the AWSs at (a) and (c) 0800 LST; (b) and (d) 1400 LST on HHR days (left), and non-HHR days (right) during the warm seasons of 2007–2014. Note that the legends for HHR days (left) and non-HHR days (right) are different.

deep convection, especially during the early afternoon period. Moreover, a long-lived or larger-scale HHR event would require the presence of a larger-scale supply of water vapour, e.g. monsoonal air, moist low-level jets.

To validate the above conjecture, Figure 11(a) compares between HHR days and non-HHR days the vertical profiles of the averaged temperature anomalies, specific humidity anomalies, and horizontal winds at 0800 LST at the Beijing observatory (see Figure 1 for its location). It is evident that the HHR (non-HHR) days were characterized with about 2 °C warmer (0.6 °C colder) than the averaged conditions from the surface to 300 hPa. More importantly, the lowest layer, i.e. below 925 hPa, indicated statically unstable (stable) conditions in temperature anomalies on the mornings of HHR (non-HHR) days (Figure 11(a) and b), with south- to southwesterly (northwesterly) flows from 925 hPa to 700 hPa. In addition, higher specific humidity occurred in the deep troposphere, especially in the lower levels, on HHR days than that on non-HHR days. The mean convective available potential energy (CAPE) on the HHR days is ~770 J kg$^{-1}$ whereas it is ~180 J kg$^{-1}$ on the non-HHR days. The above all suggested the presence of favourable larger-scale conditions on HHR days compared to those occurring on non-HHR days.

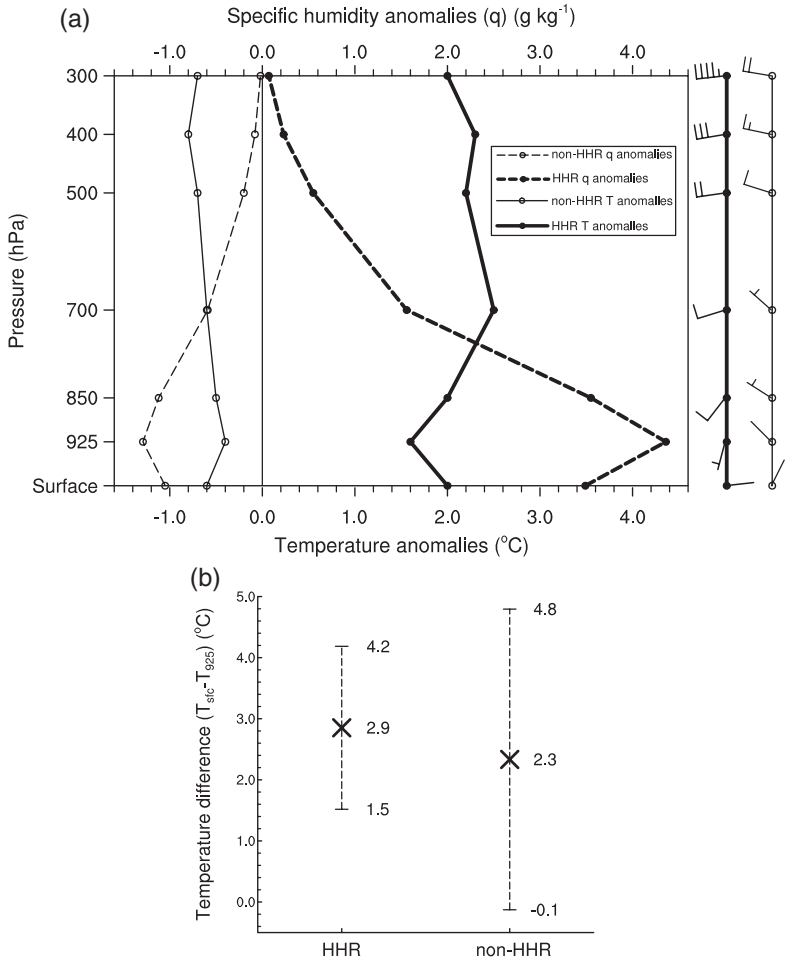


Figure 11. (a) Vertical profiles of averaged temperature anomalies (solid lines), specific humidity anomalies (dashed lines), and winds (a full barb is 4 m s$^{-1}$) of HHR days (thick lines and thick wind barbs) and non-HHR days (thin lines and thin wind barbs). The anomalies of HHR (non-HHR) days are obtained by subtracting the averaged values of HHR (non-HHR) days from the averaged values of all the days during the warm seasons of 2007–2014. (b) Difference between temperature at the surface and at the 925-hPa level (Tsfc-T925) for HHR days (left) and non-HHR days (right). The crosses mark the averaged values, and the error bars give ±1 standard deviation.

With the above presentation of the averaged surface and upper-air conditions, we may discuss their possible influences on the HHR events shown in the preceding sections. While some HHR events, e.g. occurring over the central urban regions, were correlated with local surface conditions, some were likely associated with thunderstorms moving across the plain regions during the afternoon and evening hours (see red-dashed lines in Figure 8(b)). They appear to account for the different frequencies of HHR events occurring between the central urban districts and the west and northwest mountains. Based on statistical analysis of several-year radar data covering the BMR, Chen *et al.* (2012) and Wang *et al.* (2014) indicated that convective initiation is frequent over the foothills and plains. On the other hand, some thunderstorms or MCSs propagating from the BMR's west or northwest might be apt to intensify when reaching the central urban districts due to the presence of a favourable environment (Chen *et al.*, 2012, 2014).

As compared to the more thermally favourable region of the central urban districts, the northeast mountainous regions appear to be a more mechanically favourable region for deep convection due to the presence of pronounced mountain-plain circulations. That is, the daytime warm and moist southerly flows favour the initiation of deep convection as climbing over the northeast mountains. This flow regime appears to account for the active afternoon HHR events over the region (see plum-dashed lines in Figure 8(b)). Note that the warm-moist airstream has been heated by the upstream urban surface, the so-called upstream urbanization effects by Zhang *et al.* (2011). In contrast, during the early evening hours, down-slope flows began to dominate, and favourable convergence occurred at the foothills of the northeast mountains when the associated east- to northeasterly winds met with the weak southerly flows near the southern end of the Pinggu-Shunyi border, thus favouring the generation of HHR events. This convergence zone lasted for a longer period from 1900 to 0700 LST on HHR days, while the southerly flows near the southern end of the Pinggu-Shunyi border gradually turned to northerly and the convergence weakened after 0200 LST on non-HHR days (not shown).

In contrast to the two high-frequency HHR event regions discussed above, the west and northwest mountains were

 

much less favourable for the generation of HHR events due to the presence of relatively colder and drier air. In addition, although the regions are the favourable locations for the initiation of deep convection through mountain-plain circulations, most storms, once initiated, tended to propagate eastward across the central urban districts into the plain regions, accounting for a significant portion of the HHR events downstream. A comparison of Figures 2(a) and 8(b) and 9 and 10 suggests that the south- to southeasterly warm-moist air during the daytime could climb over certain portions of the west and northwest mountains, leading to the near-constant frequency of HHR events in the afternoon hours (see blue-dashed lines in Figure 8(b)).

## 7. Summary and concluding remarks

In this study, the spatiotemporal characteristics of HHR events and rainstorm days are examined using the quality-controlled 155 AWS observations at 5-min intervals over the BMR during the warm seasons of 2007–2014. Results show pronounced variability in the frequencies of HHR events and rainstorm days between the BMR's western mountains, eastern plains, central urban districts, and northeastern mountainous regions. High-frequency HHR events and large rainfall centres are found over eastern Haidian, and near the northeast mountains in Shunyi, Miyun and Pinggu, whereas the west and northwest mountains are the regions of low-frequency HHR events with much less rainfall amount. The rainfall amount from HHR events contributes more than 30% to the total rainfall amount during the warm seasons of 2007–2014 in eastern Haidian and near the northeast mountains.

It is found that HHR events are peaked in late July with significant less frequencies prior to June 15 and after August 15, and that HHR events start most frequently during the period from 1600 to 2000 LST with much less frequencies between 0400 and 1200 LST. From 16 June to 31 August, the northeast mountains tend to experience more HHR events than the central urban districts except during the period of 16 July–15 August when the strongest solar energy is locally received.

Several extreme HHR events at various stations are documented: a total frequency of 40 and a total rainfall amount of 1517.9 mm; an 8.75 h duration, an accumulated rainfall amount of 281.5 mm associated with a single HHR event, and the maximum rainfall intensity of 32.4 mm $(5\,\text{min})^{-1}$ and 135.7 mm $h^{-1}$. Many of the above extreme events took place over either eastern Haidian or near the northeast mountains, In addition, about 80% of the BMR's AWSs recorded HHR events during the well-known 7–21 extreme rainfall event, with the record-breaking duration of 8.75 h, a large accumulated rainfall amount of 281.5 mm and an intense hourly rainfall intensity of 103.6 mm $h^{-1}$.

A comparison of the averaged surface meteorological variables and upper-air sounding at 0800 LST between HHR and non-HHR days shows that the HHR events occurred under dominant south- to southeasterly flows of surface warm and moist air during the daytime and downslope winds of relative cold and dry air from the west and northeast mountains during the nighttime, with an unstable stratification and low-level south- to southwesterly flows, and a deep layer of higher moisture content. The above-mentioned two high-frequency HHR event regions coincide, respectively, with a distinctly warmer and moister area with favourable convergence near the central urban districts, especially in the afternoon hours, and an area of more favourable upslope lifting of the southerly warm-moist flow. Such favourable correlations between HHR events and surface conditions suggest likely the positive influences of urban environment, topographical forcing and mountain-plain circulations on the generation of HHR events over the BMR.

In conclusion, we may state that there are preferred locations, periods of a month and a day for the generation of high-frequency HHR events, which appears to be positively influenced by urban environment and mountain-plain circulations. The results have important implications to operational weather forecasters for their improved prediction of HHR events, and to city planners and emergency managers for their more focused attention to the locations and timings of high-frequency HHR events. However, the present study is limited by the use of AWSs observations and upper-air observations at a single station, which cannot fully address the interaction of urban effect, topography and other processes with larger-scale environments in the generation of HHR events. Clearly, three-dimensional high-resolution observational and modelling studies are much needed to quantify various dynamical processes leading to the generation of different HHR events. In our forthcoming articles we will examine the convective initiation of an HHR event in the BMR's central urban districts using a high-resolution numerical model.

## Acknowledgements

This work was supported by the National Basic Research Program of China (973 Program) under grant No. 2014CB441402. The authors are grateful to Beijing Meteorological Bureau for providing the observations in Beijing for the present study.

## References

Blackadar AK. 1957. Boundary layer wind maxima and their significance for the growth of nocturnal inversions. *Bull. Am. Meteorol. Soc.* **83**: 283–290.

Brooks HE, Stensrud DJ. 2000. Climatology of heavy rain events in the United states from hourly precipitation observations. *Mon. Weather Rev.* **128**: 1194–1201.

Cao W, Liang X, Zhao H, Duan X, Zhang Z. 2016. Copula-based frequency analysis and its use in hazard risk assessment of Beijing heavy rainfall. *Acta. Meteor. Sin.* **74**: 772–783.

Chen YL, Li J. 1995. Large-scale conditions favorable for the development of heavy rainfall during TAMEX IOP 3. *Mon. Weather Rev.* **123**: 2978–3002.

Chen CS, Chen WS, Deng Z. 1991. A study of a mountain-generated precipitation system in northern Taiwan during TAMEX IOP 8. *Mon. Weather Rev.* **119**: 2574–2606.

 

Chen CS, Chen YL, Liu CL, Lin PL, Chen WC. 2007. Statistics of heavy rainfall occurrences in Taiwan. *Weather Forecast.* **22**: 981–1002.
Chen M, Wang Y, Gao F, Xiao X. 2012. Diurnal variations in convective storm activity over contiguous North China during the warm season based on radar mosaic climatology. *J. Geophys. Res. Atmos.* **117**: D20115, doi: 10.1029/2012JD018158.
Chen J, Zheng Y, Zhang X, Zhu P. 2013. Distribution and diurnal variation of warm-season short-duration heavy rainfall in relation to the MCSs in China. *Acta Meteor. Sin.* **27**: 868–888.
Chen M, Wang Y, Gao F, Xiao X. 2014. Diurnal evolution and distribution of warm-season convective storms in different prevailing wind regimes over contiguous North China. *J. Geophys. Res. Atmos.* **119**: 2742–2763, doi: 10.1002/2013JD021145.
Doswell CA III, Brooks HE, Maddox RA. 1996. Flash flood forecasting: an ingredients-based methodology. *Weather Forecast.* **11**: 560–581.
Dou Y, Qu Y, Tao S, Hu B. 2008. The application of quality control procedures for real-time data from automatic weather stations. *Meteorol. Mon.* **34**: 77–81.
Houze RA Jr. 2004. Mesoscale convective systems. *Rev. Geophys.* **42**: RG4003, doi: 10.1029.2004RG000150.
Houze RA Jr, Rutledge SA, Biggerstaff MI, Smull BF. 1989. Interpretation of Doppler weather radar displays in midlatitude mesoscale convective systems. *Bull. Am. Meteorol. Soc.* **70**: 608–619.
Iwasaki H. 2012. Recent positive trend in heavy rainfall in eastern Japan and its relation with variations in atmospheric moisture. *Int. J. Climatol.* **32**: 364–374.
Iwasaki H. 2015. Increasing trends in heavy rain during the warm season in eastern Japan and its relation to moisture variation and topographic convergence. *Int. J. Climatol.* **35**: 2154–2163.
Li J, Yu R, Wang J. 2008. Diurnal variations of summer precipitation in Beijing. *Chin. Sci. Bull.* **53**: 1933–1936.
Li J, Yu R, Yuan W, Chen H. 2011. Changes in duration-related characteristics of late-summer precipitation over eastern China in the past 40 years. *J. Clim.* **24**: 5683–5690.
Liu HZ, Wang WG, Shao MX, Wang XR. 2007. A case study of the influence of the western Pacific subtropical high on the torrential rainfall in Beijing area. *Chin. J. Atmos. Sci.* **31**: 727–734.
Liu W, You H, Ren G, Yang P, Zhang B. 2014. Subtle precipitation characteristics in Beijing area. *Clim. Environ. Res.* **19**: 61–68.
Luo Y, Gong Y, Zhang DL. 2014. Initiation and organizational modes of an extreme-rain-producing mesoscale convective system along a Mei-Yu front in east China. *Mon. Weather Rev.* **142**: 203–221.
Miao S, Chen F, Lemone MA, Tewari M, Li Q, Wang Y. 2009. An observational and modeling study of characteristics of urban heat island and boundary layer structures in Beijing. *J. Appl. Meteorol. Climatol.* **48**: 484–501.
Ren Z, Zhao P, Zhang Q, Zhang Z, Cao L, Yang Y, Zou F, Zhao Y, Zhao H, Chen Z. 2010. Quality control procedures for hourly precipitation data from automatic weather stations in China. *Meteorol. Mon.* **36**: 123–132.
Ren Z, Zhang Z, Sun C, Liu Y, Li J, Ju X, Zhao Y, Li Z, Zhang W, Li H, Zeng X, Ren X, Liu Y, Wang H. 2015. Development of three-step quality control system of real-time observation data from AWS in China. *Meteorol. Mon.* **41**: 1268–1277.
Sun JS, Yang B. 2008. Meso-$\beta$scale torrential rain affected by topography and the urban circulation. *Chin. J. Atmos. Sci.* **32**: 1352–1364.
Sun JS, Wang H, Wang L, Liang F, Kang YX, Jiang XY. 2006. The role of urban boundary layer in local convective torrential rain happening in Beijing on 10 July 2004. *Chin. J. Atmos. Sci.*. **30**: 221–234.
Wang G, Wang L. 2013. Temporal and spatial distribution of short-time heavy rain of Beijing in summer. *Torrential Rain Disaster.* **32**: 276–279.
Wang Y, Qian T, Zheng Y, Tao Z. 2003. Analysis and diagnosis of a local heavy rain in Miyun county, Beijing. *J. Appl. Meteorol. Sci.* **14**: 277–286.
Wang Y, Han L, Wang H. 2014. Statistical characteristics of convective initiation in the Beijing-Tianjin region reveled by six-year radar data. *J. Meteorol. Res.* **28**: 1127–1136.
Wilson JW, Chen M, Wang Y, Wang L. 2007. Nowcasting thunderstorms for the 2008 summer Olympics. In *33rd International Conference on Radar Meteorology*. American Meteorological Society: Australia.
Yang P, Liu W. 2013. Evaluating the quality of meteorological data measured at automatic weather stations in Beijing during 1998–2010. *Adv. Meteorol. Sci. Technol.* **3**: 27–34.
Yang P, Ren G, Hou W, Liu W. 2013. Spatial and diurnal characteristics of summer rainfall over Beijing municipality based on a high-density AWS dataset. *Int. J. Climatol.* **33**: 2769–2780.
Yang P, Xiao Z, Shi W. 2016. Fine-scale characteristics of rainfall in Beijing urban area based on a high-density AWS dataset. *Chin.. J. Atmos. Sci.*, doi: 10.3878/j.issn.1006-9895.1606.16134.
Yin S, Li W, Chen D, Jeong JH, Guo W. 2011. Diurnal variations of summer precipitation in the Beijing area and the possible effect of topography and urbanization. *Adv. Atmos. Sci.* **28**: 725–734.
Zhang H, Zhai P. 2011. Temporal and spatial characteristics of extreme hourly precipitation over eastern China in the warm season. *Adv. Atmos. Sci.* **28**: 1177–1183.
Zhang DL, Zheng WZ. 2004. Diurnal cycles of surface winds and temperatures as simulated by five boundary-layer parameterizations. *J. Appl. Meteorol.* **43**: 157–169.
Zhang DL, Shou YX, Dickerson RR. 2009. Upstream urbanization exacerbates urban heat island effects. *Geophys. Res. Lett.* **36**: L24401, doi: 10.1029/2009GL041082.
Zhang DL, Shou YX, Dickerson RR, Chen F. 2011. Impact of upstream urbanization on the urban heat island effects along the Washington-Baltimore corridor. *J. Appl. Meteorol. Climatol.* **50**: 2012–2029.
Zhang W, Wang Y, Cui X, Chen M. 2012. Analysis of a local rain storm in Beijing associated with two convective lines. *J. Trop. Meteorol.* **28**: 873–887.
Zhang DL, Lin Y, Zhao P, Yu X, Wang S, Kang H, Ding Y. 2013. The Beijing extreme rainfall of 21 July 2012: 'Right results' but for wrong reasons. *Geophys. Res. Lett.* **40**: 1426–1431, doi: 10.1002/grl.50304.
Zheng Z, Qi W, Li Q, Li L. 2015. Statistical characteristics of precipitation in summer in Beijing area during 2007–2011. *Clim. Environ. Res.* **20**: 201–208.
Zhong L, Mu R, Zhang DL, Zhao P, Zhang Z, Wang N. 2015. An observational analysis of warm-sector rainfall characteristics associated with the 21 July 2012 Beijing extreme rainfall event. *J. Geophys. Res. Atmos.* **120**: 3274–3291, doi: 10.1002/2014JD022686.

 